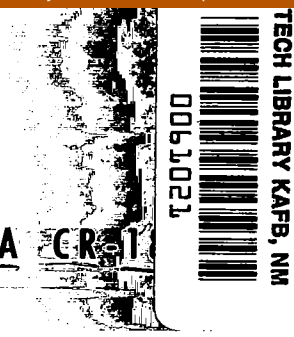

NASA CONTRACTOR REPORT

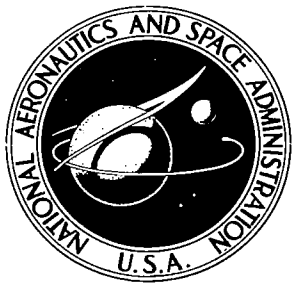

NASA CR-1865

NUMERICAL STUDY OF AXISYMMETRIC VORTEX BREAKDOWNS

by K. E. Torrance and R. M. Kopecky

Prepared by
CORNELL UNIVERSITY
Ithaca, N.Y. 14850
for Lewis Research Center

NATIONAL AERONAUTICS AND SPACE ADMINISTRATION • WASHINGTON, D. C. • AUGUST 1971

1. Report No.	2. Government Accession No.	3. Recipient's Catalog No.
NASA CR-1865		

4. Title and Subtitle	5. Report Date
NUMERICAL STUDY OF AXISYMMETRIC VORTEX BREAKDOWNS	August 1971
	6. Performing Organization Code
7. Author(s)	8. Performing Organization Report No.
K. E. Torrance and R. M. Kopecky	None
	10. Work Unit No.
9. Performing Organization Name and Address	
Cornell University Ithaca, New York 14850	11. Contract or Grant No.
	NGL 33-010-064
	13. Type of Report and Period Covered
12. Sponsoring Agency Name and Address	Contractor Report
National Aeronautics and Space Administration Washington, D.C. 20546	14. Sponsoring Agency Code

15. Supplementary Notes

16. Abstract

Axisymmetric flow of a rotating stream is analyzed to determine conditions which will allow an isolated eddy (vortex breakdown) to develop. The eddy represents a fluid region totally confined by the external stream. The effects of axial velocity, swirl distribution, and viscosity on eddy formation are systematically explored with the aid of numerical solutions of the governing dynamic equations. These solutions also provide the structure of the flow inside and outside of the eddy. The structure is displayed with figures illustrating streamline contours for two inlet geometries. Ranges of axial flow Reynolds number and swirl ratio are determined which lead to confined eddies.

17. Key Words (Suggested by Author(s))	18. Distribution Statement
Fluid mechanics Vortex breakdown Fluid confinement	Unclassified - unlimited

19. Security Classif. (of this report)	20. Security Classif. (of this page)	21. No. of Pages	22. Price*
Unclassified	Unclassified	37	$3.00

* For sale by the National Technical Information Service, Springfield, Virginia 22151

FOREWORD

The research described in this report was conducted at Cornell University under NASA grant NGL 33-010-064 with Dr. John C. Evvard of the Lewis Research Center as the NASA Project Manager.

SUMMARY

Axisymmetric flow of a rotating stream is analyzed to determine conditions which will allow an isolated eddy (vortex breakdown) to develop. The eddy represents a fluid region totally confined by the external stream. The effects of axial velocity, swirl distribution, and viscosity on eddy formation are systematically explored with the aid of numerical solutions of the governing dynamic equations. These solutions also provide the structure of the flow inside and outside of the eddy. The structure is displayed with figures illustrating streamline contours for two inlet geometries. Ranges of axial flow Reynolds number and swirl ratio are determined which lead to confined eddies.

INTRODUCTION

Experiments have shown that swirling fluid streams can support internal, closed eddies when the swirl is sufficiently large. Such a phenomenon offers a possibility for fluid confinement without using solid boundaries. The objective of the present study is to examine the feasibility of fluid confinement by this mechanism.

Backflows in rotating fluids moving axially through diverging cross sections have been observed by several workers [5, 6, 8]. The flow exhibits a stagnation point and reversed velocity on the axis, and is appropriately called a "vortex breakdown". The otherwise ordinary vortex flow breaks down when the axial pressure gradient becomes large enough to drive secondary backflows.

The breakdown phenomenon was isolated from other flows by Harvey [10], who employed a vortex tube. In his experiments, the breakdown appeared as a small, bubble-like region of confined flow on the axis when the swirl exceeded a critical value. The breakdown extended both upstream and downstream with an increase in swirl until the whole length of the tube was filled with a central core region with reversed axial velocity. As the size of the viscous core of the upstream swirl flow was reduced the diameter of the breakdown bubble became smaller. Harvey measured the swirl angle profile just upstream of a vortex breakdown bubble; this profile is used as input to parts of the present study. The internal structure of the breakdown was not studied experimentally because conventional probes disturb the breakdown and cause it to migrate to the probe. The vortex breakdown phenomenon has also been observed in other flow configurations [4, 11, 17, 18, 20].

Analytic studies of the vortex breakdown fall in two categories: those that are primarily concerned with the cause and prediction of the phenomenon; and those that are concerned with the structure of the breakdown flow. Results from the first category lead to reasonably accurate predictions of the phenomenon provided the swirl flow upstream of the breakdown is known. The analyses considered inviscid flow [1, 15, 23] or boundary layer-type flow [9]. In the second category are several studies of the structure of inviscid breakdowns [3, 7, 16]. Velocity perturbations were introduced to initiate the eddy. Also, a numerical study allowing for viscous effects was undertaken by

Lavan, et al. [13] to obtain the structure of the breakdown for low Reynolds number (Re) flows (Re based on radius less than 20).

The present study employs numerical solutions of the dynamic equations to obtain the structure of the flow inside and outside the vortex breakdown for a wide range of operating conditions. No approximations in different regions of the flow are used; and no assumption that vortex breakdown is an inviscid phenomenon is made. This study also attempts to determine the region, on a map of Reynolds number versus the amount of swirl, where a vortex breakdown will form.

FORMULATION OF THE PROBLEM

Swirling flows within a straight and circular streamtube of constant cross-sectional area are examined. A cylindrical coordinate system (x, r, θ) is appropriate and is sketched in figure 1. The streamtube radius is r_o. The velocity components are denoted by u, v, and w for the axial, radial, and azimuthal directions. Two configurations for the entering flow are considered as shown in figure 2. In one, fluid enters axially and in the other, radially. Viscous flows are examined for both inlets, and inviscid flows are also considered for the axial inlet. Throughout, the flows are assumed to be axisymmetric and incompressible.

Viscous Flow Equations

The fluid motion is governed by three time dependent momentum equations and a mass continuity equation. By multiplying the θ-momentum equation by r, an equation for the transport of circulation T is obtained. Circulation may be identified with angular momentum and is given by $T = rw$. The x- and r-momentum equations can be cross-differentiated to eliminate pressure, and an equation for the transport of aximuthal vorticity Ω results.

Appropriate scaling parameters are the tube radius, r_o, the mean axial velocity in the tube, U, and an angular velocity ω_o. The latter will typically be taken as the angular velocity of the tube wall at the inlet. Denoting dimensional variables with primes, corresponding nondimensional variables become:

$$t = \frac{U}{r_o} t', \quad x = \frac{x'}{r_o}, \quad r = \frac{r'}{r_o}$$

$$u = \frac{u'}{U}, \quad v = \frac{v'}{U}, \quad w = \frac{w'}{r_o \omega_o} \tag{1}$$

$$\psi = \frac{\psi'}{r_o^2 U}, \quad T = \frac{T'}{r_o^2 \omega_o}, \quad \Omega = \frac{r_o}{U} \Omega' .$$

The resulting nondimensional equations are:†

$$\frac{\partial T}{\partial t} + \frac{\partial (uT)}{\partial x} + \frac{1}{r}\frac{\partial (rvT)}{\partial r} = \frac{1}{Re}\left[\frac{\partial^2 T}{\partial x^2} + r\frac{\partial}{\partial r}\left(\frac{1}{r}\frac{\partial T}{\partial r}\right)\right] \tag{2a}$$

$$\frac{\partial \Omega}{\partial t} + \frac{\partial (u\Omega)}{\partial x} + \frac{\partial (v\Omega)}{\partial r} = 2\Gamma^2 \frac{T}{r^3}\frac{\partial T}{\partial x} + \frac{1}{Re}\left[\frac{\partial^2 \Omega}{\partial x^2} + \frac{\partial}{\partial r}\left(\frac{1}{r}\frac{\partial (r\Omega)}{\partial r}\right)\right] \tag{2b}$$

$$\frac{1}{r}\frac{\partial^2 \psi}{\partial x^2} + \frac{\partial}{\partial r}\left(\frac{1}{r}\frac{\partial \psi}{\partial r}\right) = -\Omega \tag{2c}$$

$$u = \frac{1}{r}\frac{\partial \psi}{\partial r}\,, \quad v = -\frac{1}{r}\frac{\partial \psi}{\partial x}\,, \quad w = \frac{T}{r}\,. \tag{2d}$$

Equation (2c) is provided by the definition of vorticity and the first two of equations (2d) by the definition of stream function.

The nondimensional transport equations for the circulation T and the azimuthal vorticity Ω introduce two independent parameters into the problem, the Reynolds number (Re) and the swirl ratio (Γ) defined as

$$Re = \frac{U r_o}{\nu} \quad \text{and} \quad \Gamma = \frac{r_o \omega_o}{U}\,. \tag{3}$$

The Reynolds number is the ratio of inertial forces to viscous forces; the swirl ratio is the ratio of the characteristic rotational speed to the characteristic axial speed. It is apparent from equations (2) that the essential dependent variables governing the viscous, axisymmetric flow of an incompressible fluid are T, Ω and ψ. Velocities can be expressed in terms of ψ and T through equations (2d). The dependent variables are functions of the coordinates x and r, time t, and the parameters Re and Γ.

Inviscid Flow Equation

In the absence of viscous effects, circulation T and vorticity Ω are simply convected along with the flow. Thus, only the stream function relation (2c) need be retained. For the steady flow of an inviscid, rotational fluid, the stream function equation becomes††

$$-r\left[\frac{1}{r}\frac{\partial^2 \psi}{\partial x^2} + \frac{\partial}{\partial r}\left(\frac{1}{r}\frac{\partial \psi}{\partial r}\right)\right] = \Gamma^2 T \frac{dT}{d\psi} - r^2 \frac{dP}{d\psi} \tag{4}$$

† Except for the source terms and the nondimensional parameters, these equations are similar to those used by Torrance [24].

†† See Squire [22] for derivation.

where all variables are dimensionless and P is the dimensionless total pressure ($P = P'/\rho U^2$). In contrast to the previous section, only one equation is now involved. The dependent variable is ψ, and as the total derivatives indicate, T and P are functions only of ψ. Prescriptions for the $T - \psi$ and $P - \psi$ relations are required and come from the boundary conditions.

Initial Data and Boundary Conditions

Viscous flow. - The circulation and vorticity transport equations (2a) and (2b) are written in time dependent form. Such a coupled system (they are coupled through the circulation term in equation 2b) is more readily solved numerically when posed as an initial-value rather than as a boundary-value (or time steady) problem. In addition, the time dependent form allows solutions which may be hydrodynamically unsteady. Only time steady vortex breakdowns were observed in the present study, but there was no reason to anticipate this in advance. Initial conditions in the streamtube were taken to be either: a uniform, parallel flow with an arbitrary swirl distribution; or the steady flow from another run which used different values of Re and Γ. Final results were independent of which initial condition was used.

Boundary conditions on the streamtube must be prescribed and are essential for establishing a confined eddy. The two flow configurations considered are illustrated in figure 2; the axial inlet (figure 2a) will be discussed first. Fluid enters the tube with a uniform axial velocity (u) and a prescribed radial distribution of swirl velocity (w). The swirl velocity profile is taken to be of exponential vortex form:

$$w = \frac{1}{r}\left(1 - e^{-Br^2}\right) \tag{5}$$

where B denotes a constant. Such a distribution is a good description of a viscous vortex, and was verified by Harvey [10] to exist upstream of a vortex breakdown bubble.† Since a number of experimental configurations could be expected to generate such a profile, it appears to be a realistic choice for the inlet stream.

The profile given by equation (5) is shown in figure 3(a) for values of $B = 8$ and 14. These are the values employed in the present study; with the latter corresponding to Harvey's experiments. The vortex displays solid body rotation near the axis ($w \propto r$) and free vortex behavior far from the axis ($w \propto r^{-1}$). The exponential vortex is displayed in terms of the dependent variables in figure 3(b) as circulation T versus ψ. For uniform flow at the inlet, $\psi = r^2/2$. A free vortex corresponds to $T = 1$, and it is apparent that the viscous core is larger for $B = 8$ than for $B = 14$.

† Harvey actually measured a swirl angle distribution. The swirl angle ϕ is related to the dimensionless velocities by $\phi = \tan^{-1}(\Gamma w/u)$. If the axial velocity is constant with r, equation (5) can be used to obtain the swirl angle distribution.

At the wall of the streamtube (figure 2 a) boundary conditions were selected so as to isolate the flow dynamics as much as possible from the influence of containing walls. In particular, a zero axial shear surface is employed to eliminate the effect of developing wall boundary layers. Also, the confining streamtube is presumed to rotate at a constant speed w = 1. This matches the inlet condition, so that a fluid particle at r = 1 neither gains or loses angular momentum as it moves down the streamtube (i.e., T = 1). These conditions simulate flow within the entrance of a real tube (rotating or stationary) as long as the wall boundary layers are thin and the core flow at entrance matches the inlet profile of this study.

The remaining boundary conditions are common to both inlet configurations. The axis (r = 0) is a line of zero shear and zero angular momentum ($\Omega = T = 0$); the stream function is assigned the value $\psi = 0$. The total volume rate of flow through the streamtube is then equal to π. The volume rate of flow per radian in the θ-direction becomes $\psi = \pi/2\pi = 0.5$, and this is the ψ-value assigned to r = 1. The tube is assumed to be long enough so that axial variations at the tube exit are small. Accordingly all dependent variables employed the condition $\partial/\partial x = 0$ there. Justification for this condition follows from the boundary layer equations which are expected to be valid far downstream. These equations neglect axial diffusion and require only one boundary condition in the x-direction, that at the inlet. Thus the boundary condition at the end of the tube plays the role of a "weak" condition (not essential) and its actual form ($\partial/\partial x = 0$) is not expected to have an important effect on the flow.

Boundary conditions on T, Ω and ψ for the axial inlet may be summarized as follows:

$$
\begin{array}{ll}
r = 0, \quad \text{all } x & T = \Omega = \psi = 0 \\
r = 1, \quad \text{all } x & T = 1, \quad \Omega = 0, \quad \psi = 0.5 \\
x = 0, \quad \text{all } r & T = 1 - e^{-Br^2}, \quad \Omega = 0, \quad \psi = \dfrac{r^2}{2} \\
x = \text{tube exit, all } r & \dfrac{\partial T}{\partial x} = \dfrac{\partial \Omega}{\partial x} = \dfrac{\partial \psi}{\partial x} = 0 \ .
\end{array}
\qquad (6)
$$

For the radial inlet (figure 2 b), fluid enters the tube along r = 1 between x = 0 and 1 with a uniform radial velocity v = - 0.5 and a uniform swirl velocity w = 1. Downstream, the tube rotates at angular velocity w = 1 and wall boundary layers are allowed to develop in the axial direction. That is, wall shear is included. This arrangement should simulate physical experiments more closely than the axial inlet because the swirl profile is allowed to develop naturally. The inlet could be achieved with a porous ring on the tube or by a radial swirl vane entrance as in the experiments of Harvey.

Boundary conditions for the radial inlet are as follows:

$$
\begin{array}{ll}
r = 0, \quad \text{all } x & T = \Omega = \psi = 0 \\
r = 1, \quad 0 \leq x < 1.0 & T = 1, \quad \Omega = 0, \quad \psi = \dfrac{x}{2}
\end{array}
\qquad (7)
$$

$r = 1, \quad x \geq 1.0$	$T = 1, \quad \frac{\partial \psi}{\partial r} = 0, \quad \psi = 0.5$
$x = 0, \quad$ all r	$\frac{\partial T}{\partial x} = 0, \quad \Omega = 0, \quad \psi = 0$
x = tube exit, all r	$\frac{\partial T}{\partial x} = \frac{\partial \Omega}{\partial x} = \frac{\partial \psi}{\partial x} = 0.$

(7)

Conditions at x = 0 correspond to a zero-shear plane of symmetry, which can be realized in practice by constructing a mirror-image flow for x < 0 rotating in the same sense. Secondary flows arising from a rigid wall at x = 0 are thereby avoided.† An examination of vortex behavior independent of such side effects was sought. Note that vorticity at the wall cannot be expressed explicitly, but can be determined from stream function boundary conditions in the course of the numerical solutions, as will be explained later.

Inviscid flow. - For an inviscid fluid, the governing equation (4) requires two boundary conditions on ψ for each of the x- or r-directions, as well as relationships for total pressure P and circulation T in terms of ψ. The latter relationships could be determined for the axial inlet but not for the radial inlet, and the inviscid calculations were thus restricted to the axial inlet configuration. Appropriate ψ-boundary conditions are:

$r = 0, \quad$ all x	$\psi = 0$
$r = 1, \quad$ all x	$\psi = 0.5$
$x = 0, \quad$ all r	$\psi = r^2/2$
x = tube exit, all r	$\frac{\partial \psi}{\partial x} = 0$.

(8)

Circulation T and total pressure P are convected downstream without change from the inlet along streamlines. Therefore, conditions at the inlet may be employed to evaluate T and P. For the axial inlet, the radial momentum balance requires

$$\frac{\partial p}{\partial r} = \Gamma^2 \frac{T^2}{r^3} \tag{9}$$

where all variables are dimensionless and p is the static pressure ($p = p'/\rho U^2$). The latter is related to the total pressure P by

$$P = p + \frac{1}{2}(u^2 + v^2 + \Gamma^2 w^2) \ . \tag{10}$$

† Secondary flows in jet-driven vortex tubes have been observed by Rosenzweig, Lewellen and Ross [19] in which the end-wall boundary layers are primarily responsible for the strong axial flows existing in the vortex.

This can be rewritten as

$$\frac{dP}{d\psi} = \frac{\partial p}{\partial r}\frac{dr}{d\psi} + \frac{1}{2} r^2 \frac{d(w^2)}{d\psi}$$
$$= r^2 \frac{1}{2\psi} T \frac{dT}{d\psi} \qquad (11)$$

using $T = wr$, $\psi = r^2/2$, and equation (9). The right side of the governing equation (4) becomes

$$(1 - \frac{r^2}{2\psi}) r^2 T \frac{dT}{d\psi} \qquad (12)$$

and only a $T - \psi$ relation remains to be specified. This is taken to be the exponential vortex which reduces (using $\psi = r^2/2$ at the inlet) to

$$T = 1 - e^{-2B\psi} \quad \text{for } \psi \geq 0 . \qquad (13a)$$

Fluid eddies with $\psi < 0$ could not originate at the inlet in a steady flow ($\psi \geq 0$ there), but a definition of their T-values must be prescribed in case an eddy develops. For convenience, such fluid elements are assigned the values

$$T = -(1 - e^{2B\psi}) \quad \text{for } \psi < 0 . \qquad (13b)$$

The rotational sense is opposite to that in the inlet. It is worth noting that the solutions are unaffected by the rotational sense of the eddies relative to the inlet since only the product $T\, dT/d\psi$ appears in relation (12).

NUMERICAL METHOD

Grid System

Numerical methods, suitable for digital computation, are developed which permit solutions of the flow equations. For most of the calculations, the flow field is partitioned into a uniform, rectangular grid. The x and r location of any grid point in terms of its i and j coordinates is given by $x = (i - 1)\Delta x$ and $r = (j - 1)\Delta r$ where Δx and Δr are the grid dimensions and i and j are the integers 1, 2, 3, etc. The value of a quantity like circulation or azimuthal vorticity at a grid point is the average of the quantity over a small rectangle with dimensions Δx by Δr centered about the grid point. At any instant in time this grid point quantity is constant throughout a ring of fluid with radius r and cross-sectional dimensions Δx by Δr. The transport of a quantity from grid point to grid point is approximated by a finite difference scheme.

For the axial inlet, a grid size of 22 mesh points in the x-direction and 11 mesh points in the r-direction (22 by 11) was used. The streamtube was 5.25 dimensionless units long and 1.00 units in radius, so that $\Delta x = 0.25$ and $\Delta r = 0.1$. For the radial inlet, a grid size of 12 mesh points in the x-direction and 6 mesh points in the r-direction (12 by 6) was used. The streamtube was 5.50 units long and 1.00 units in radius, so that $\Delta x = 0.50$ and $\Delta r = 0.2$. A finer grid, 22 by 11, and a variable mesh grid with a transformation for an infinitely long tube were also used for a few solutions of the radial inlet configuration.

Finite Difference Scheme for the Viscous Flow Equations

The set of viscous flow equations (2a-d) that govern the fluid confinement problem are solved by the method of finite differences. All linear space derivatives are approximated by three point central differences. The nonlinear space derivatives of the form $\partial(uF)/\partial x$ are approximated by special three point noncentral differences. For the grid point (i,j) the method is as follows:

$$\left(\frac{\partial(uF)}{\partial x}\right)_{i,j} \doteq \frac{1}{\Delta x}\left(\frac{u_{i,j} + u_{i+1,j}}{2} F_{i,j} - \frac{u_{i-1,j} + u_{i,j}}{2} F_{i-1,j}\right) \qquad (13)$$

when the coefficients $(u_{i,j} + u_{i+1,j})/2$ and $(u_{i-1,j} + u_{i,j})/2$ are positive and

$$\left(\frac{\partial(uF)}{\partial x}\right)_{i,j} \doteq \frac{1}{\Delta x}\left(\frac{u_{i,j} + u_{i+1,j}}{2} F_{i+1,j} - \frac{u_{i-1,j} + u_{i,j}}{2} F_{i,j}\right) \qquad (14)$$

when the coefficients are negative. For one coefficient positive and one coefficient negative the appropriate term from equation (13) and the appropriate term from equation (14) are used. The difference scheme is constructed so as to fully satisfy mass, circulation, and vorticity conservation within the grid system. Additional details and discussions of the stability, convergence, and conservation properties are provided by Torrance [24].

The calculation proceeds from a known flow configuration of T, Ω and ψ at time t (which may be the initial data) by explicitly extrapolating to time level $t' = t + \Delta t$ the T and Ω fields at all interior points. All space differences are evaluated at time t. A forward difference approximation is used for the time derivative. Circulation is advanced first using a finite difference approximation of equation (2a),

$$T'_{i,j} = \Delta t \left[\left[\frac{1}{Re(\Delta x)^2}\right]T_{i+1,j} + \left[\frac{\bar{u}_{i-1,j}}{\Delta x} + \frac{1}{Re(\Delta x)^2}\right]T_{i-1,j} \right.$$

$$+ \left[\frac{1}{\Delta t} - \frac{\bar{u}_{i,j}}{\Delta x} - \frac{(1 + \frac{\Delta r}{2r})}{\Delta r}\bar{v}_{i,j} - \frac{2}{Re(\Delta x)^2} - \frac{2}{Re(\Delta r)^2}\right]T_{i,j} \qquad (15)$$

$$\left. + \left[\frac{1 - \frac{\Delta r}{2r}}{Re(\Delta r)^2}\right]T_{i,j+1} + \left[\frac{1 - \frac{\Delta r}{2r}}{\Delta r}\bar{v}_{i,j-1} + \frac{(1 + \frac{\Delta r}{2r})}{Re(\Delta r)^2}\right]T_{i,j-1} \right] .$$

Equation (15) is written for the case when the mean velocities ($\bar{u}_{i,j} = (u_{i,j} + u_{i+1,j})/2$) are positive.

The azimuthal vorticity is next advanced using a finite difference approximation to equation (2b),

$$\Omega'_{i,j} = \Delta t \left[\left[\frac{1}{Re(\Delta x)^2}\right]\Omega_{i+1,j} + \left[\frac{\bar{u}_{i-1,j}}{\Delta x} + \frac{1}{Re(\Delta x)^2}\right]\Omega_{i-1,j} \right.$$

$$+ \left[\frac{1}{\Delta t} - \frac{\bar{u}_{i,j}}{\Delta x} - \frac{\bar{v}_{i,j}}{\Delta r} - \frac{2}{Re(\Delta x)^2} - \left(\frac{1}{1 + \frac{\Delta r}{2r}} + \frac{1}{1 - \frac{\Delta r}{2r}}\right)\frac{1}{Re(\Delta r)^2}\right]\Omega_{i,j} \qquad (16)$$

$$+ \left[\frac{1 + \frac{\Delta r}{r}}{1 + \frac{\Delta r}{2r}}\frac{1}{Re(\Delta r)^2}\right]\Omega_{i,j+1} + \left[\frac{\bar{v}_{i,j-1}}{\Delta r} + \frac{1 - \frac{\Delta r}{r}}{1 - \frac{\Delta r}{2r}}\frac{1}{Re(\Delta r)^2}\right]\Omega_{i,j-1}$$

$$\left. + 2\Gamma^2 \frac{T}{r^3}\frac{T'_{i+1,j} - T'_{i-1,j}}{2\Delta x} \right]$$

Again, this is written for the case when the mean velocities are positive. Note that the last term is evaluated at the new time level and is constant over the time step.

In order to bring ψ up-to-date with the new values of T and Ω, equation (2c) must be solved. This is accomplished by approximating it with finite differences, and solving the resulting set of simultaneous equations by the iterative technique of optimized successive over-relaxation. A new iterate at level (s + 1) is determined from values at level (s) using

$$\psi_{i,j}^{(s+1)} = (1 - \omega_b)\psi_{i,j}^{(s)}$$

$$+ \frac{\omega_b}{\frac{2}{(\Delta x)^2} + \frac{1}{(1 + \frac{\Delta r}{2r})(\Delta r)^2} + \frac{1}{(1 - \frac{\Delta r}{2r})(\Delta r)^2}} \left[r\Omega'_{i,j} \right. \tag{17}$$

$$+ \frac{1}{(\Delta x)^2}\psi_{i+1,j}^{(s)} + \frac{1}{(\Delta x)^2}\psi_{i-1,j}^{(s+1)} + \frac{1}{(1 + \frac{\Delta r}{2r})(\Delta r)^2}\psi_{i,j+1}^{(s)}$$

$$\left. + \frac{1}{(1 - \frac{\Delta r}{2r})(\Delta r)^2}\psi_{i,j-1}^{(s+1)} \right] .$$

An optimum relaxation factor, ω_b, can be computed for a given grid size; the details are given by Smith [21]. For the grids used in this study, a maximum of fifteen iterations (always sweeping in the same direction) was used. Less than fifteen iterations were used if the ratio of the maximum value of $|\psi_{i,j}^{(s+1)} - \psi_{i,j}^{(s)}|$ for all the grid points to the maximum value of $|\psi_{i,j}^{(s)}|$ in the field is less than 5×10^{-6}.

Certain of the boundary conditions must still be considered. The requirement of $\partial/\partial x = 0$ at the tube exit is satisfied by adding an extra column of grid points with field variables identical to the last computed column of grid points. The circulation at the plane of symmetry (radial inlet) is computed from a finite difference approximation of equation (2a) which incorporates the symmetry conditions. The wall vorticity (radial inlet) is determined from the up-dated stream function field as follows: At the wall, the stream function is constant and the axial velocity u is zero (no-slip condition). The vorticity equation therefore reduces to $\Omega = -\partial^2\psi/\partial r^2$. A Taylor series expansion for ψ leads to a first order approximation of the wall vorticity,

$$\Omega_o = -\frac{2(\psi_1 - \psi_o)}{(\Delta r)^2} , \tag{18}$$

where the subscripts 0 and 1 denote the wall and one grid point away from the wall, respectively.

The velocities u, v, and w are determined from equations (2d) using three point central difference approximations for the derivatives. All field variables are now known and current at time $t' = t + \Delta t$. Before repeating the numerical procedure for the next time advancement, a value for the time step Δt is determined from stability considerations.

The numerical method is stable (in the sense of Lax and Richtmyer [14])

if Δt is suitably restricted. No constraints are imposed on the spatial mesh increments. Stability requires that the sum of the absolute values of the coefficients of equations (15) and (16) be bounded by unity. Such a bound exists if all the coefficients are positive, and this can be guaranteed if Δt satisfies an inequality of the following form at all interior grid points:

$$\Delta t \leq \left[\frac{\bar{u}_{i,j}}{\Delta x} + \left(1 + \frac{\Delta r}{2r}\right) \frac{\bar{v}_{i,j}}{\Delta r} + \frac{2}{Re(\Delta x)^2} + \frac{2}{1 - \left(\frac{\Delta r}{2r}\right)^2} \frac{1}{Re(\Delta r)^2} \right]^{-1} . \quad (19)$$

Suitable permutations of the velocity are employed in this expression if the mean velocities are negative, or a mixture of positive and negative. Because the difference equations are consistent with the governing partial differential equations, Lax and Richtmyer stability implies that the numerical solutions will converge to the exact solution of the differential equations as Δt, Δx and Δr tend to zero.

The size of the time step given by inequality (19) decreases with decreasing Reynolds number (Re). Results indicate that flow transients also take more time, t, as Re increases. Computation of a steady state flow for the axial inlet at Re = 100, 200 and 1000 respectively required approximately 300, 700 and 2000 time advancements. Since the latter is directly proportional to the amount of computer time required, computations were restricted to Re $\leq$ 1000 for the axial inlet. Similar results were observed for the radial inlet, but because a coarser grid was generally employed, Re was restricted to $\leq$ 3000. Of course, quantitative results at very high Re may require refining the spatial grids beyond those of the present study.

Finite Difference Scheme for the Inviscid Flow Equation

The finite difference approximation of the inviscid flow equation is identical to equation (17) except that $r\Omega'_{i,j}$ is replaced by

$$\left[1 - \frac{r^2}{2\psi_{i,j}}\right] r^2 \left(T \frac{dT}{d\psi}\right)_{i,j} \quad (20)$$

and a Jacobi advancement is used ($\omega_b = 1$ and all iteration levels on the right hand side of equation (17) become s). For stability of the inviscid fluid calculations it was necessary to use 75 and 50 percent of the Jacobi advancement of the stream function field for B = 8 and B = 14. The initial field was usually taken to be a uniform, swirling flow with an axial perturbation. The number of ψ-iterations required depended upon whether or not the final field had a vortex breakdown. With a breakdown, about 1000 iterations were required; without a breakdown, about 200.

RESULTS

A steady, confined eddy of fluid that exhibits flow reversal along the axis will be called a vortex breakdown. It may be helpful at this point to examine figures 4, 5, 6, and 7 which show streamline fields containing vortex breakdowns. The location of these streamlines was determined by cross plotting the computed values at the mesh points. In each of the streamline plots the centerline of the cylindrical streamtube is shown on the bottom; the entrance to the streamtube is to the left and the exit to the right. The abscissa is the axial coordinate x, and the ordinate is the radial coordinate r.

This investigation covers a range of Reynolds numbers from 50 to infinity (the inviscid case) for the axial inlet and from 10 to 3000 for the radial inlet. For the axial inlet, the results are believed to have quantitative validity, and yield the general flow field as well as the shape, size, strength, and location of a vortex breakdown if it appears. Results for the inviscid fluid are compared to the results for the viscous fluid when the Reynolds number is large. For the radial inlet, only qualitative trends about the formation of the vortex breakdown can be inferred, for reasons to be discussed later.

Axial Inlet-Viscous Flow

The development of a vortex breakdown with variations in Reynolds number or swirl ratio may be conveniently examined with the aid of figures 4 and 5. Results pertain to an exponential swirl distribution in the axial inlet with $B = 8$. All graphs portray the steady state streamline fields. The streamlines represent the intersection of an axial plane with the various streamtubes given by ψ = constant. The actual streamlines are helical paths traced out on these tubes.

Results shown in these figures (and throughout this report) were obtained by advancing the transient solution procedure in time from some initial field until steady flows were achieved. In all cases, the transient evolution was smooth. Vortex breakdowns appeared or disappeared quite naturally, without oscillations or random motions of the breakdown or supporting stream. Multiple breakdowns within the flow did not appear. Consequently, primary attention here will be directed to the final, steady flows.

Figure 4 illustrates the breakdown development with increasing swirl at a fixed Reynolds number, $Re = 100$. In figure 4(a) the amount of swirl, $\Gamma = 0.752$, is not enough to cause a stagnation point along the axis. However, the respective diffluence and confluence of the streamlines suggest that an eddy may be forming. As the swirl is increased to $\Gamma = 0.833$, figure 4(b), an eddy does indeed form within the flow. This eddy is closed and has a forward and rearward stagnation point. The size and shape of the vortex breakdown is defined by the streamline with value zero. As the swirl ratio is increased further to $\Gamma = 0.909$, figure 4(c), the vortex breakdown becomes larger in size and stronger. The forward stagnation point moves forward while the rearward stagnation point moves rearward. The location of the maximum absolute value of stream function inside the vortex breakdown migrates forward

slightly, and its magnitude increases from 1.0×10^{-3} to 4.7×10^{-3}. Nearly five times as much fluid is now undergoing reversed flow in figure 4(c) as compared to figure 4(b).

As the swirl ratio is increased further to $\Gamma = 1.25$, figure 4(d), the vortex breakdown grows distinctively larger in the radial direction and extends out the tube in the axial direction. For a very large swirl ratio, $\Gamma = 10$, figure 4(e) shows that the breakdown almost completely fills the streamtube. Field variables near the inlet change rapidly in the x-direction for $\Gamma = 1.25$ and 10, suggesting that a real breakdown would tend to migrate upstream and alter the upstream boundary conditions.

Figure 5 illustrates the breakdown development with increasing Reynolds number. The swirl ratio is held constant, $\Gamma = 0.833$. The trends in figure 5 are strikingly similar to those in figure 4. For Re = 50, no breakdown appears but the streamlines suggest that one is imminent. As the Reynolds number is increased to 100 and to 200, a vortex breakdown develops and increases in size and strength. This increase of Reynolds number moves the location of the maximum absolute value of stream function inside the vortex breakdown upstream and it increases in magnitude from 1.0×10^{-3} to 3.5×10^{-3}. For Re = 500 the breakdown extends out the tube.

Figure 6 portrays a breakdown at a higher Reynolds number, Re = 1000, also with B = 8. Clearly, the breakdown is now greatly elongated and very slim. The swirl ratio for this breakdown ($\Gamma = 0.714$) is very near that for which a breakdown first appears ($\Gamma = 0.697$). Calculations suggest that a breakdown near $\Gamma = 0.697$ will also extend out the tube at this Reynolds number. The flow in figure 6 is similar to the bore flows observed by Benjamin and Barnard [2], in which the main flow is water but the cavity is filled with air.

Figure 7 illustrates the breakdown development with increasing swirl for a different inlet swirl distribution, B = 14. In this figure, the Reynolds number is held fixed at Re = 100. The viscous core becomes smaller as B is increased, and for vortex breakdowns of similar strength, those for B = 14 are more slender than those for B = 8. Figures 4(b) and 7(b) both have a breakdown strength of $\psi = -1.0 \times 10^{-3}$, but the maximum radius of the breakdown for B = 8 is 0.26 units while that for B = 14 is 0.22 units. Similarly, the breakdowns shown in Figures 4(c) and 7(c) are of nearly the same strength, but the maximum radius of the breakdown for B = 8 is 0.34 while that for B = 14 is 0.30.

For all of the streamline plots except those showing a breakdown going out the end of the tube, or nearly going out, the streamlines near the end of the tube change very little in the x-direction. Thus, the tube is long enough so that the boundary condition $\partial/\partial x = 0$ is satisfied. When the breakdown extends out the tube, this condition is not nearly so well satisfied.

By selecting a value of Re and varying Γ or by selecting a value of Γ and varying Re, it is possible to determine a critical value, Γ_c or Re_c, at which a vortex breakdown will appear. The locus of the points thus determined separates a region of flows with breakdowns from a region without breakdowns, and will be called the incipient breakdown line. Such a line is shown in

The amount of swirl required for an incipient breakdown decreases as the Reynolds number increases and an asymptotic value of swirl ratio is approached for large Reynolds number.

The vortex breakdowns in the radial inlet streamtube are similar in shape to those for the axial inlet. As either the swirl ratio or the Reynolds number is increased, the forward stagnation point moves upstream and the rearward stagnation point moves downstream. With increasing swirl, the location of the maximum absolute value of stream function inside the vortex breakdown moves upstream, but with increasing Reynolds number, the location moves downstream. The latter result is contrary to that observed with the axial inlet.

Near the incipient breakdown condition a vortex breakdown forms just downstream of the inlet ($x > 1$) as a small isolated eddy. As the forward stagnation point migrates upstream with increasing Γ or Re, the question naturally arises of whether or not it will reach $x = 0$. Since the boundary conditions applied at $x = 0$ postulate a mirror-image flow for $x < 0$, migration of the eddy up to $x = 0$ corresponds to the merging of separate eddies (one for $x > 0$ and one for $x < 0$) to form a single eddy symmetric about $x = 0$.

Since the 12 x 6 grid could not adequately answer the aforementioned question, a sequence of runs was initiated using successively refined grids for Re = 100, $\Gamma = 1.0$. Results are shown in figure 14. Figure 14(a) corresponds to the 12 x 6 grid, figure 14(b) to a 22 x 11 grid, and figure 14(c) to a 22 x 11 variable mesh grid in an infinitely long tube. The latter was achieved by introducing a coordinate transformation and is described in an appendix to a thesis by Kopecky [12]. Dashed streamlines indicate regions where interpolation is uncertain.

The eddy is basically similar for all three grids, and extends up to and includes the first computable mesh point (for figures 14(a), (b) and (c) this was $x = 0.5$, $r = 0.2$; $x = 0.25$, $r = 0.1$; and $x = 0.25$, $r = 0.065$). It appears that the breakdown does actually merge with its mirror-image counterpart. This has not been observed in the experiments cited. Typically, a contoured wall at $x = 0$ with a spiked centerbody along the axis was employed. This wall appears to be important for setting up the swirl profile in the tube, but its inclusion in a numerical simulation is not yet possible. Thus, the boundary condition along $x = 0$ fails to fully simulate experiments, but it does suggest a new way in which an eddy may be confined. By injecting fluid through a radial inlet in the middle of a long tube it may be possible to fix the location of a vortex breakdown to $x = 0$, $r = 0$. Further work is needed to determine if the breakdown will remain centered as it grows axially with increases in either Re or Γ.

Some observations on an optimum grid size may be deduced from figure 14. Results are all qualitatively very similar. Quantitatively, the grid of figure 14(b) appears to adequately describe the structure and magnitude of the breakdown circulation. The bulge near $x = 1$ does not appear in the other flows because they employ somewhat coarser axial grids in that region. [The grid of figure 14(b) was employed for all of the axial inlet calculations. Its adequacy for that geometry was verified by a run using Re = 50, $\Gamma = 1$ and a 42 x 21 grid. Results differed from the 22 x 11 grid generally by only a few percent.] It appears that the 12 x 6 grid of figure 14(a), coupled with

the singular nature of the breakdown itself, limits us to a qualitative discussion. Extensive streamline fields for the grid were computed but are not presented.

The foregoing observations are supported by an additional grid refinement for conditions very near the onset of a breakdown. A 12 x 6 grid at Re = 100, $\Gamma = 0.714$ yielded a flow with a diffluence and confluence of streamlines that suggested a breakdown was imminent, but it was not present. A grid of 22 x 11, however, yielded a weak vortex breakdown for these conditions that extended along the axis in the inlet region. Such behavior is due to truncation errors, which cause the numerical solutions to correspond to values of Re and Γ which may be shifted slightly from the input values. For conditions near the critical Γ_c, this can lead to the results just noted since the breakdown develops rapidly with Γ, as shown in figure 10.

CONCLUSIONS

Numerical solutions, which are exact in the sense that no terms in the governing differential equations were neglected, have been obtained for isolated eddies confined in a rotating stream. Two types of inlets to a straight and circular stream tube of constant cross-sectional area were investigated (see figure 2).

Results for the axial inlet yield quantitative information on the general flow field as well as the detailed structure and location of a vortex breakdown (if it appears). The most important findings may be summarized as follows:

(a) The development or initiation of a vortex breakdown with variations in Re or Γ is indicated by a sequence of streamline plots (see, for instance, figures 4 and 5).

(b) The incipient breakdown conditions (figure 8) reveal that a critical swirl ratio is required to achieve a vortex breakdown. This ratio decreases with increasing Re and attains an asymptotic value.

(c) There appears to be no hysterisis mechanism controlling the vortex breakdown in a viscous fluid, i.e., the breakdown appears and disappears for the same value of Γ.

(d) The breakdown grows in size in both the axial and radial direction when either Re or Γ is increased.

(e) The location of the maximum absolute value of stream function inside the vortex breakdown migrates forward slightly and increases in strength for an increase in either Re or Γ. The upstream migration of the breakdown is limited by the imposed inlet conditions.

(f) The breakdown strength is very sensitive to changes in the amount of swirl near the incipient or critical value (see figure 10).

(g) For the same strength vortex breakdowns at a given Re, the smaller the viscous core at the tube axis the slimmer the breakdown.

(h) A comparison between the inviscid flow calculations and the viscous flow calculations for large Reynolds number (Re > 1000) indicates that viscosity may be important for closing the vortex breakdown (providing a rear stagnation point) and confining the breakdown to within a finite tube length.

Some of the above observations are reinforced by Harvey's work. Related to (b), he found that a steady vortex breakdown forms above some critical value of swirl angle. His experiments were performed at Re $\simeq$ 4300 with an inlet swirl profile described by B = 14. The corresponding critical swirl ratio is Γ_c = 0.49, which compares quite favorably with the asymptotes given in figure 8. Related to (c), Harvey found that the breakdown can occur as a smooth and reversible transition. Related to (d), he found that with an increase in swirl the breakdown grows axially in both the upstream and downstream directions until, eventually, the whole length of the streamtube is filled with a central core region with axial velocity reversal. And related to (g) he found that the smaller the viscous core at the tube centerline, the smaller the diameter of the breakdown bubble. Although the latter comparisons are necessarily qualitative, the observations of Harvey generally support the results of this investigation.

For fluid confinement purposes it is necessary that the vortex breakdown have a rear stagnation point. This study indicates that for a straight and circular streamtube of constant cross-sectional area a rear stagnation point does not exist for Reynolds number large, i.e., as the fluid becomes inviscid. The photographs by Harvey [10] and Cassidy and Falvey [4] of vortex breakdowns in this type of streamtube for large Reynolds numbers (Re > 4000) also do not indicate a rear stagnation point. Instead, the tail of the vortex breakdown appears to be an elongated helical vortex that precesses unsteadily about the tube centerline. Thus, as conclusion (h) states, viscosity and/or tube length may be important for closing the breakdown.

For the radial inlet the calculations indicate that the breakdown wants to form in the inlet. Thus, it may be possible to confine a vortex breakdown to one location by having the fluid enter radially through a porous section of rotating tube and exit axially in opposite directions.

The above overall study indicates that the vortex breakdown phenomenon is amenable to detailed observation when the method of finite differences is used to solve the governing differential equations cast in terms of circulation, azimuthal vorticity, and stream function. The approach to the problem of fluid confinement by means of vortex breakdown could use the techniques outlined herein along with any experimental measurements of the breakdown's flow field that can be obtained. It may then be possible to incorporate the vortex breakdown phenomenon in a design for high temperature energy production.

REFERENCES

1. Benjamin, T. B., "Theory of the Vortex Breakdown Phenomenon", J. Fluid Mech., 14, p. 593, 1962.

2. Benjamin, T. B. and Barnard, B. J. S., "A Study of the Motion of a Cavity in a Rotating Liquid", J. Fluid Mech., 19, p. 193, 1964.

3. Bossel, H. H., "Vortex Breakdown Flowfield", Phys. Fluids, 12, p. 498, 1969.

4. Cassidy, J. J. and Falvey, H. T., "Observations of Unsteady Flow Arising after Vortex Breakdown", J. Fluid Mech., 41, p. 727, 1970.

5. Chanaud, R. C., "Observations of Oscillatory Motion in Certain Swirling Flows", J. Fluid Mech., 21, p. 111, 1965.

6. Chigier, N. A. and Beer, J. M., "Velocity and Static-Pressure Distributions in Swirling Air Jets Issuing from Annular and Divergent Nozzles", J. Basic Engrg., Trans. A.S.M.E., 86, p. 788, 1964.

7. Chow, C. Y., "Swirling Flow in Tubes of Non-Uniform Cross-Sections", J. Fluid Mech., 38, p. 843, 1969.

8. Gore, R. W. and Ranz, W. E., "Backflows in Rotating Fluids Moving Axially through Expanding Cross Sections", A.I.Ch.E. Journal, 10, p. 83, 1964.

9. Hall, M. G., "A New Approach to Vortex Breakdown", Proc. Heat Transfer and Fluid Mech. Inst., Stanford Univ. Press, Stanford, Calif., p. 319, 1967.

10. Harvey, J. K., "Some Observations of the Vortex Breakdown Phenomenon", J. Fluid Mech., 14, p. 585, 1962.

11. Kirkpatrick, D. L. I., "Experimental Investigation of the Breakdown of a Vortex in a Tube", Ministry of Aviation, London, C. P. No. 821, 1965.

12. Kopecky, R. M., "Numerical Study of the Structure of Vortex Breakdowns", M.S. Thesis, Cornell University, Ithaca, New York, 1971.

13. Lavan, Z., Nielsen, H., and Fejer, A. A., "Separation and Flow Reversal in Swirling Flows in Circular Ducts", Phys. Fluids, 12, p. 1747, 1969.

14. Lax, P. D. and Richtmyer, R. D., "Survey of the Stability of Linear Finite Difference Equations", Comm. Pure Appl. Math., 9, p. 267, 1956.

15. Leibovich, S., "Axially-Symmetric Eddies Embedded in a Rotational Stream", J. Fluid Mech., 32, p. 529, 1968.

16. Leibovich, S., "Weakly Non-Linear Waves in Rotating Fluids", J. Fluid Mech., 42, p. 803, 1970.

17. Lowson, M. V., "Some Experiments with Vortex Breakdown", J. Royal Aero. Society, 68, p. 343, 1964.

18. Maxworthy, T., "The Flow Creating a Concentration of Vorticity Over a Stationary Plate", JPL Space Programs Summary 37-44, 4, p. 243, 1968.

19. Rosenzweig, M. L., Lewellen, W. S. and Ross, D. H., "Confined Vortex Flows with Boundary-Layer Interaction", A.I.A.A. Journal, 2, p. 2127, 1964.

20. Sarpkaya, T., "An Experimental Investigation of the Vortex-Breakdown Phenomenon", U.S. Naval Postgraduate School, NPS-59SL0071A, Monterey, Calif., 1970.

21. Smith, G. D., Numerical Solution of Partial Differential Equations, Oxford University Press, New York, 1965.

22. Squire, H. B., Chapter on Rotating Fluids in Surveys in Mechanics, G. K. Batchelor and R. M. Davies, Eds., Cambridge University Press, London, p. 139, 1956.

23. Squire, H. B., "Analysis of the Vortex Breakdown Phenomenon", in Mizellaneen du Angewandten Mechanik, Akademie, Berlin, 1962.

24. Torrance, K. E., "Comparison of Finite-Difference Computations of Natural Convection", J. Res. of the N.B.S. - B. Math. Sciences, 72B, p. 281, 1968.

APPENDIX - SYMBOLS

t	Time
x,r,θ	Coordinates in the axial, radial, and azimuthal directions (figure 1)
u,v,w	Velocity components in the axial, radial, and azimuthal directions (figure 1)
T	Circulation or angular momentum (= rw)
Ω	Azimuthal vorticity component (equation 2c)
ψ	Stream function (equations 2d)
ρ	Density
p	Static pressure
P	Total pressure (equation 10)
ν	Kinematic viscosity
r_o	Tube radius
ω_o	Angular velocity of tube wall at the inlet
U	Average axial velocity
Re	Reynolds number (= Ur_o/ν)
Γ	Swirl ratio (= $r_o\omega_o/U$)
Re_c	Critical Re required to initiate a breakdown at constant Γ
Γ_c	Critical Γ required to initiate a breakdown at constant Re
ϕ	Swirl angle (= $\tan^{-1}[\Gamma w/u]$)
B	Adjustable constant (equation 5)

Subscripts:

i,j	Axial and radial grid indices

Superscripts:

$'$	Time level ($t' = t + \Delta t$) or dimensional variable
s	Iteration level

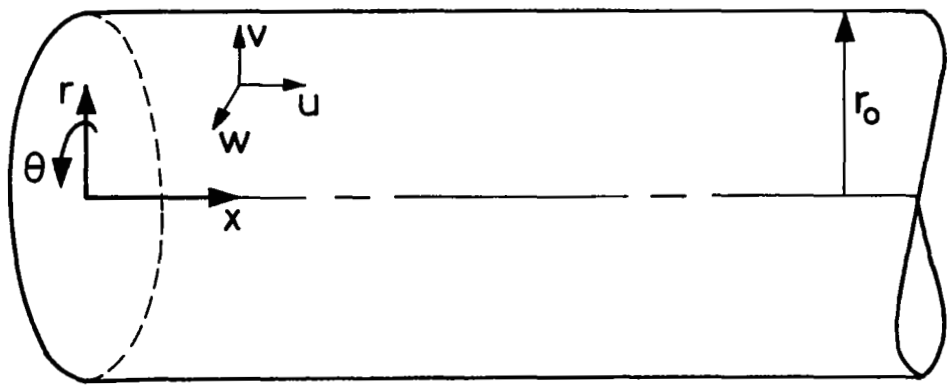

Figure 1: Stream Tube and Coordinate System.

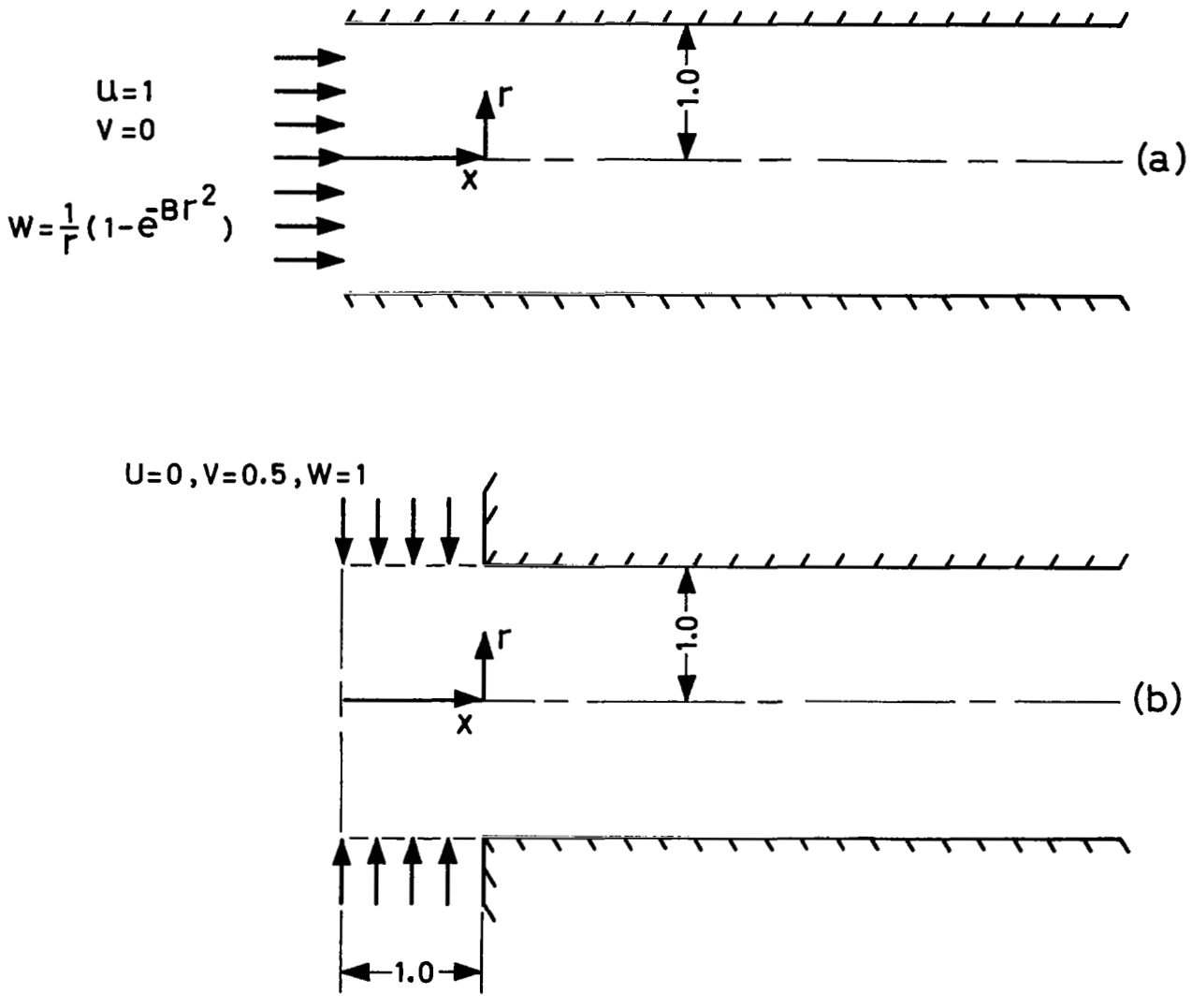

Figure 2: Inlet Configurations. (a) Axial Inlet; (b) Radial Inlet.

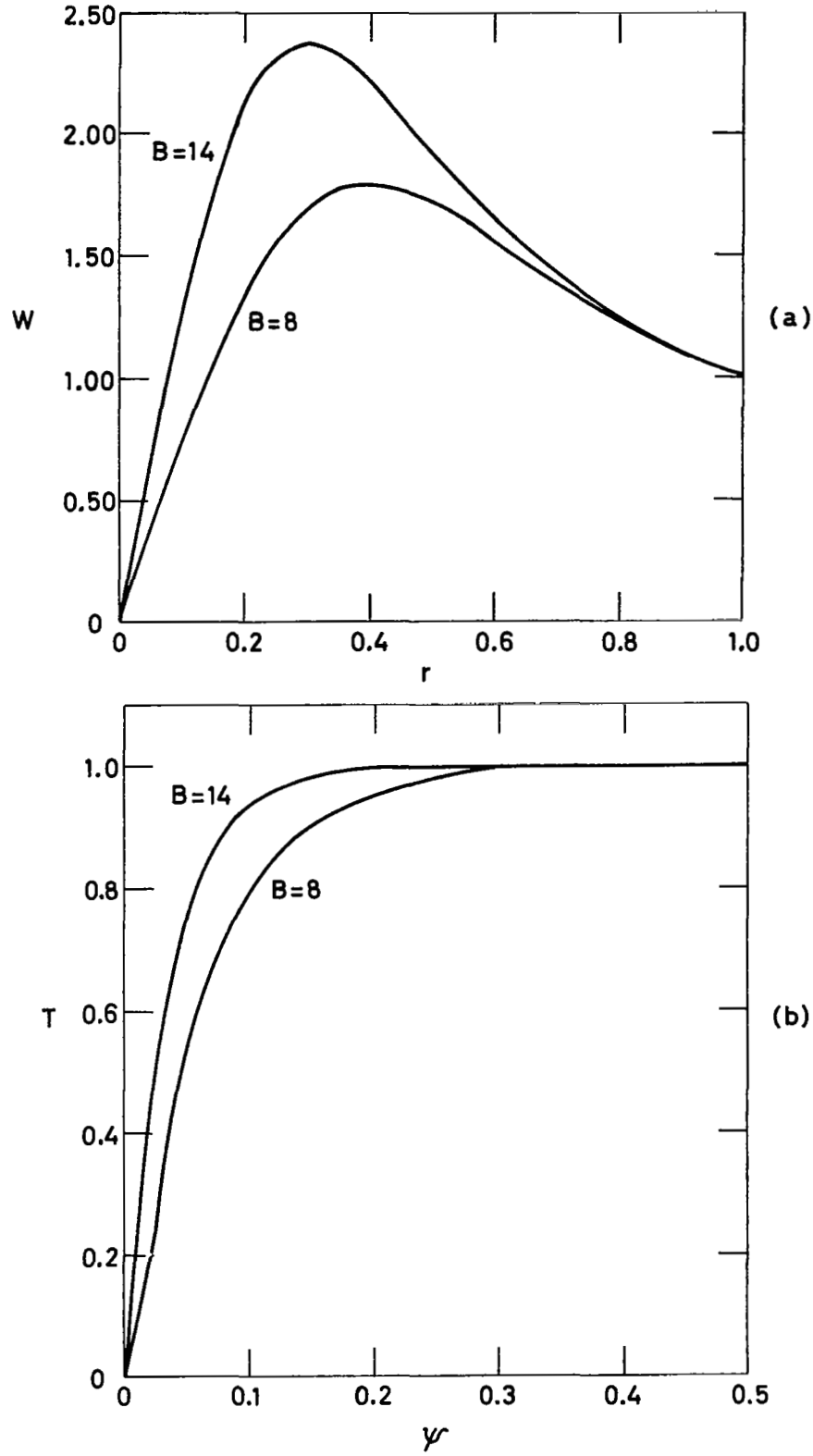

Figure 3: Swirl Distribution at the Entrance to the Axial Inlet Stream Tube. (a) Swirl Velocity Versus Radius; (b) Circulation Versus Stream Function.

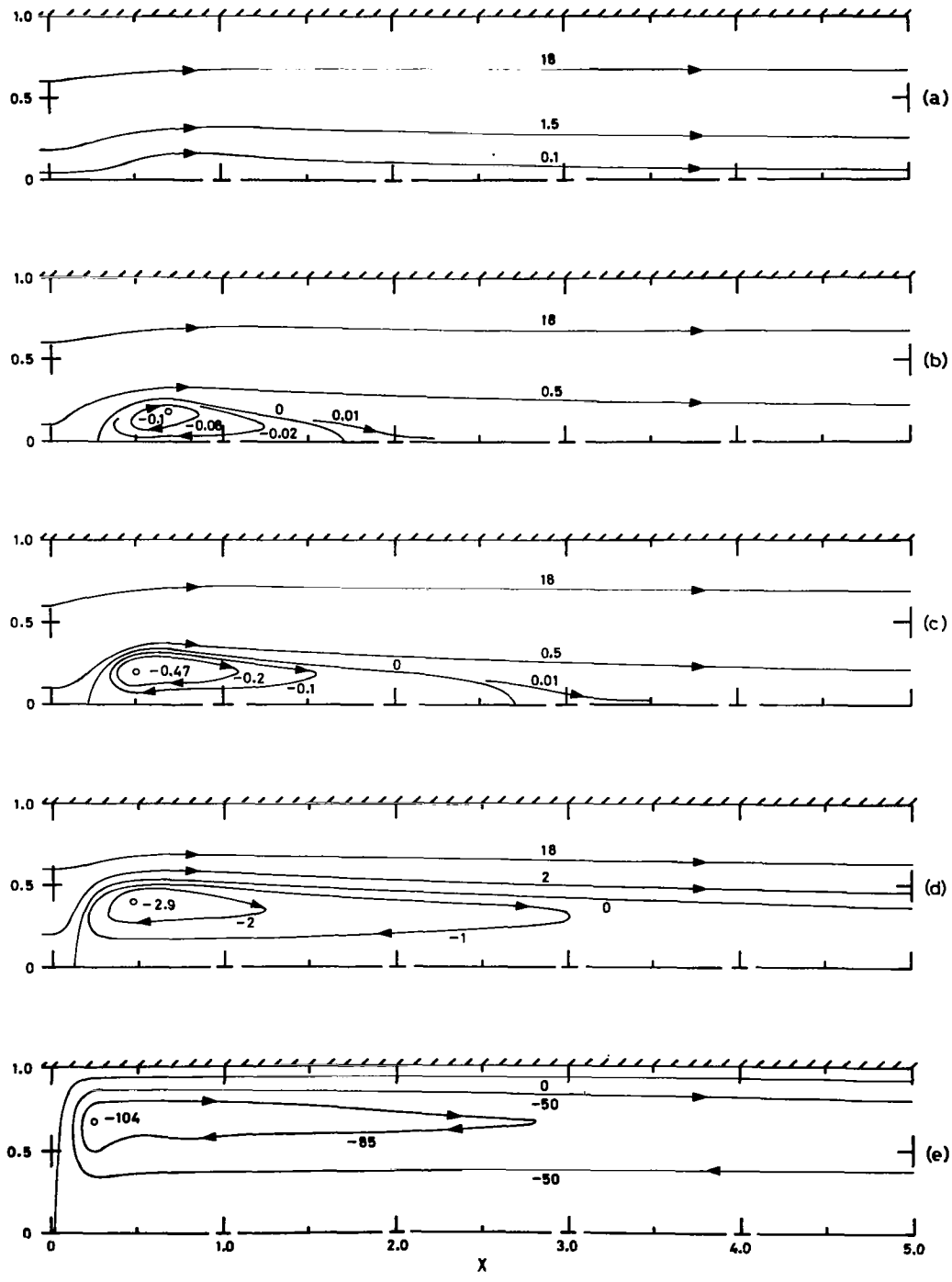

Figure 4: Development of the Vortex Breakdown with Increasing Swirl Ratio for the Axial Inlet Configuration. Re = 100 and B = 8. Stream Function Values Equal Those Shown x 10^{-2}. (a) Γ = 0.752; (b) Γ = 0.833; (c) Γ = 0.909; (d) Γ = 1.25; (e) Γ = 10.

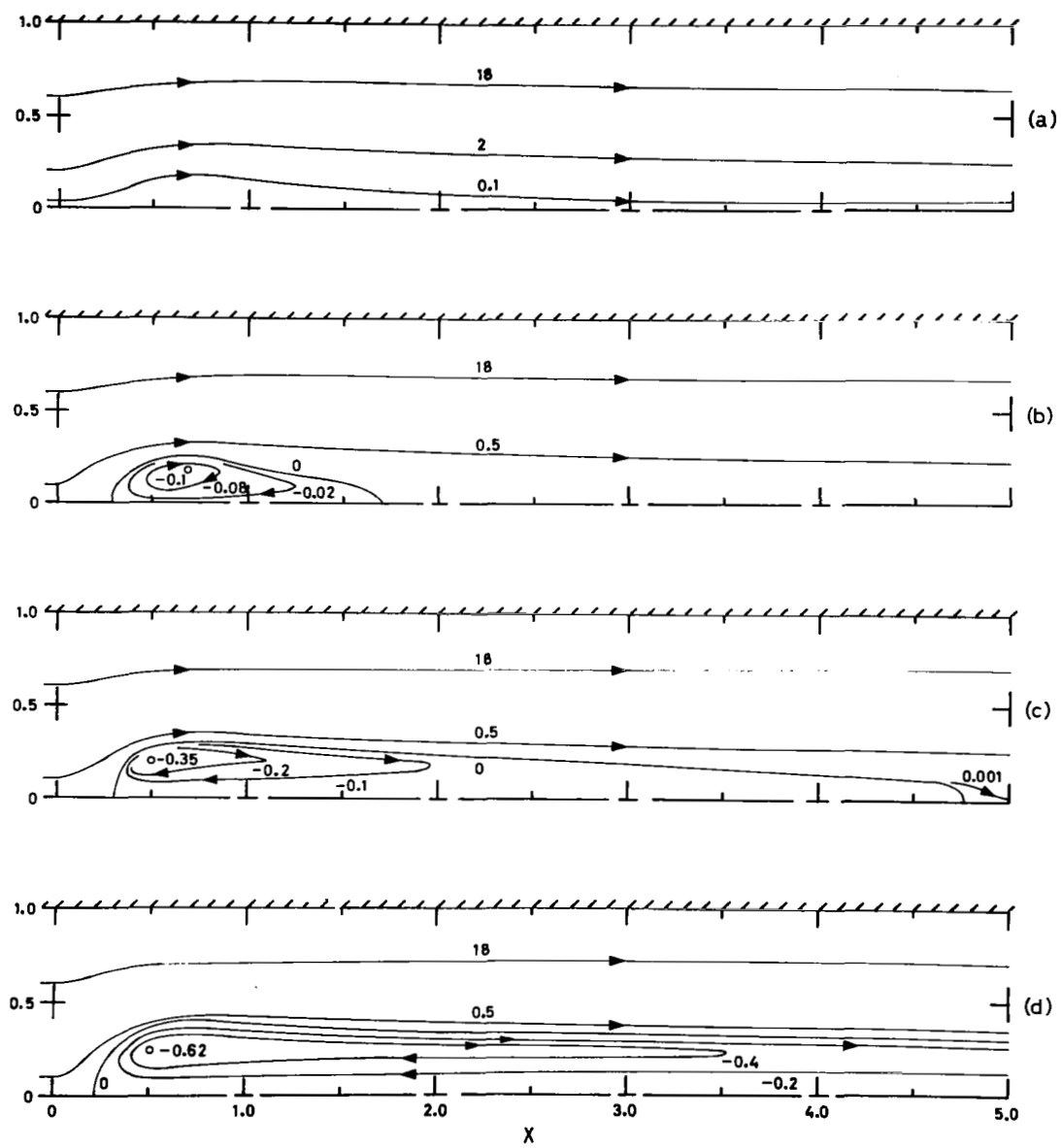

Figure 5: Development of the Vortex Breakdown With Increasing Reynolds Number for the Axial Inlet Configuration. $\Gamma = 0.833$ and $B = 8$. Stream Function Values Equal Those Shown x 10^{-2}. (a) Re = 50; (b) Re = 100; (c) Re = 200; (d) Re = 500.

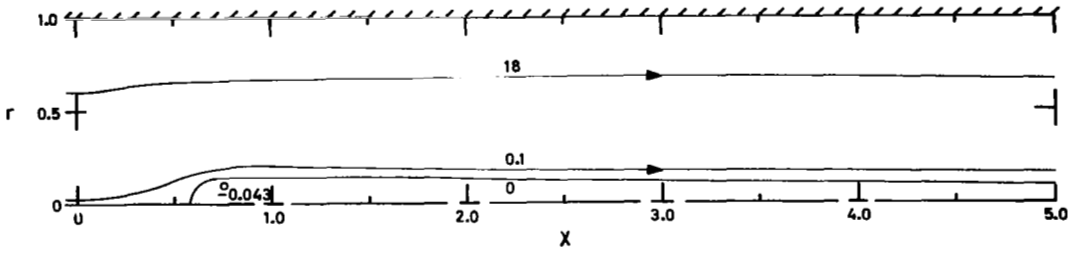

Figure 6: Vortex Breakdown Near the Critical Swirl Ratio for the Axial Inlet Configuration. Re = 1000, Γ = 0.714, and B = 8. Stream Function Values Equal Those Shown x 10^{-2}.

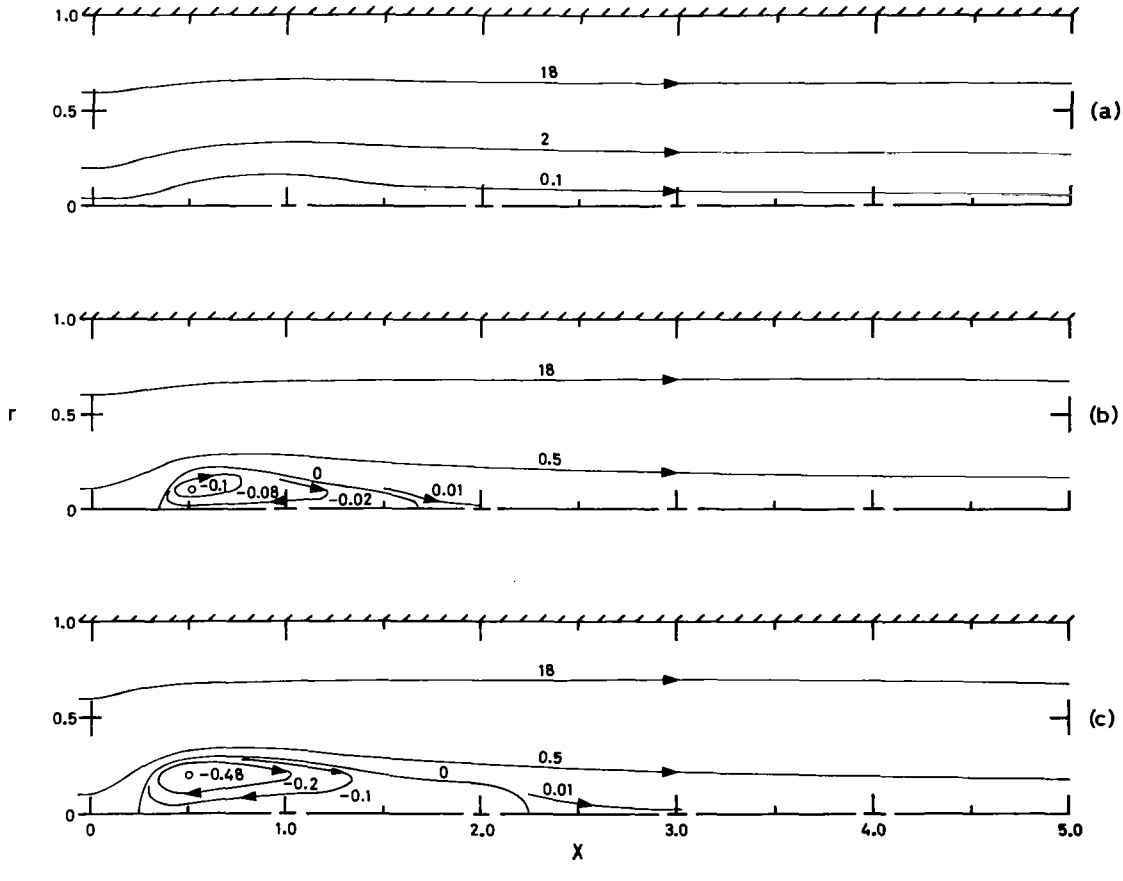

Figure 7: Development of the Vortex Breakdown With Increasing Swirl Ratio for the Axial Inlet Configuration. Re = 100 and B = 14. Stream Function Values Equal Those Shown x 10^{-2}. (a) Γ = 0.532; (b) Γ = 0.585; (c) Γ = 0.641.

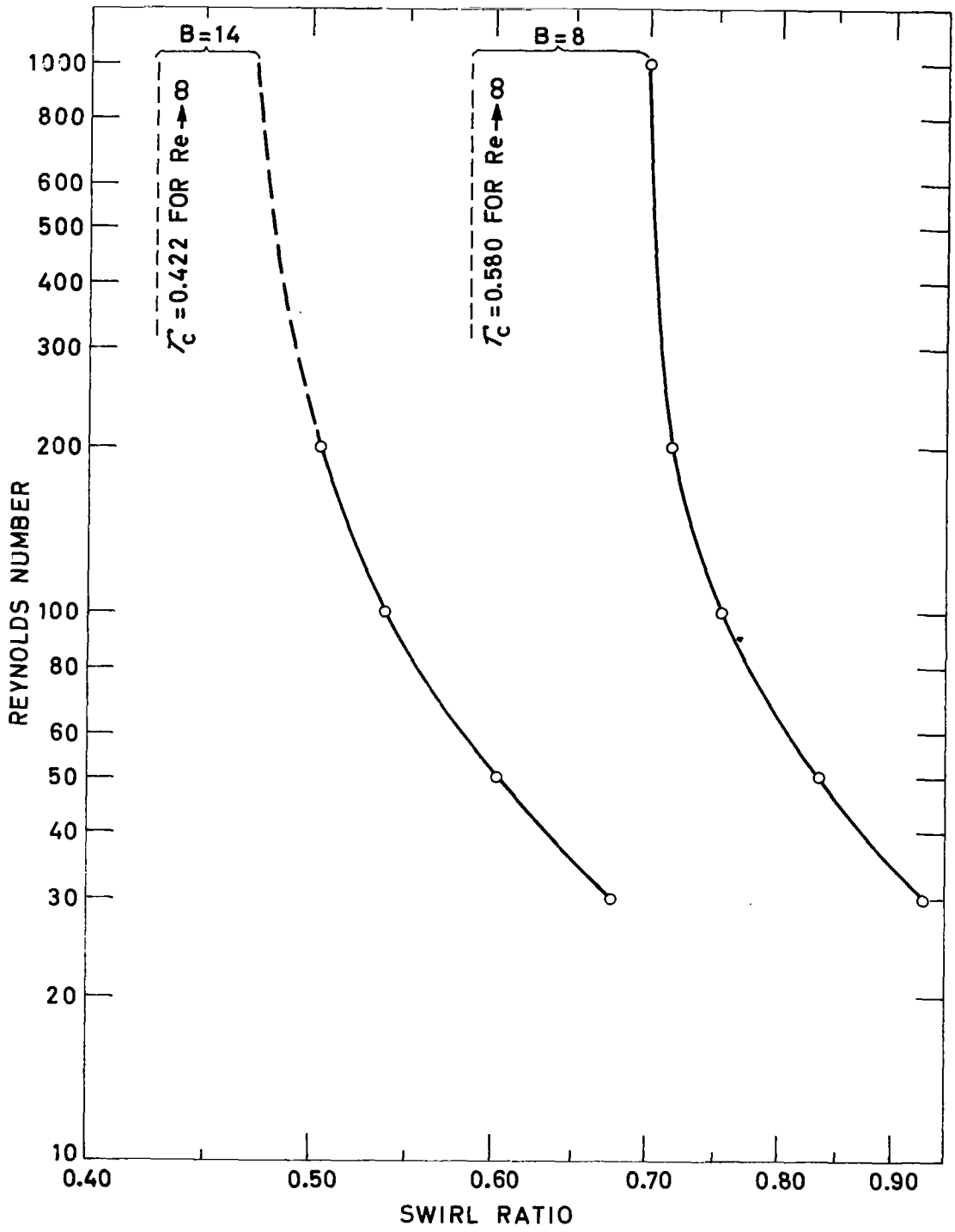

Figure 8: Swirl Ratios Required for an Incipient Breakdown at Various Reynolds Numbers. Axial Inlet Stream Tube Used. Vertical Dashed Line Indicates Critical Swirl Ratio for Inviscid Flow Calculations.

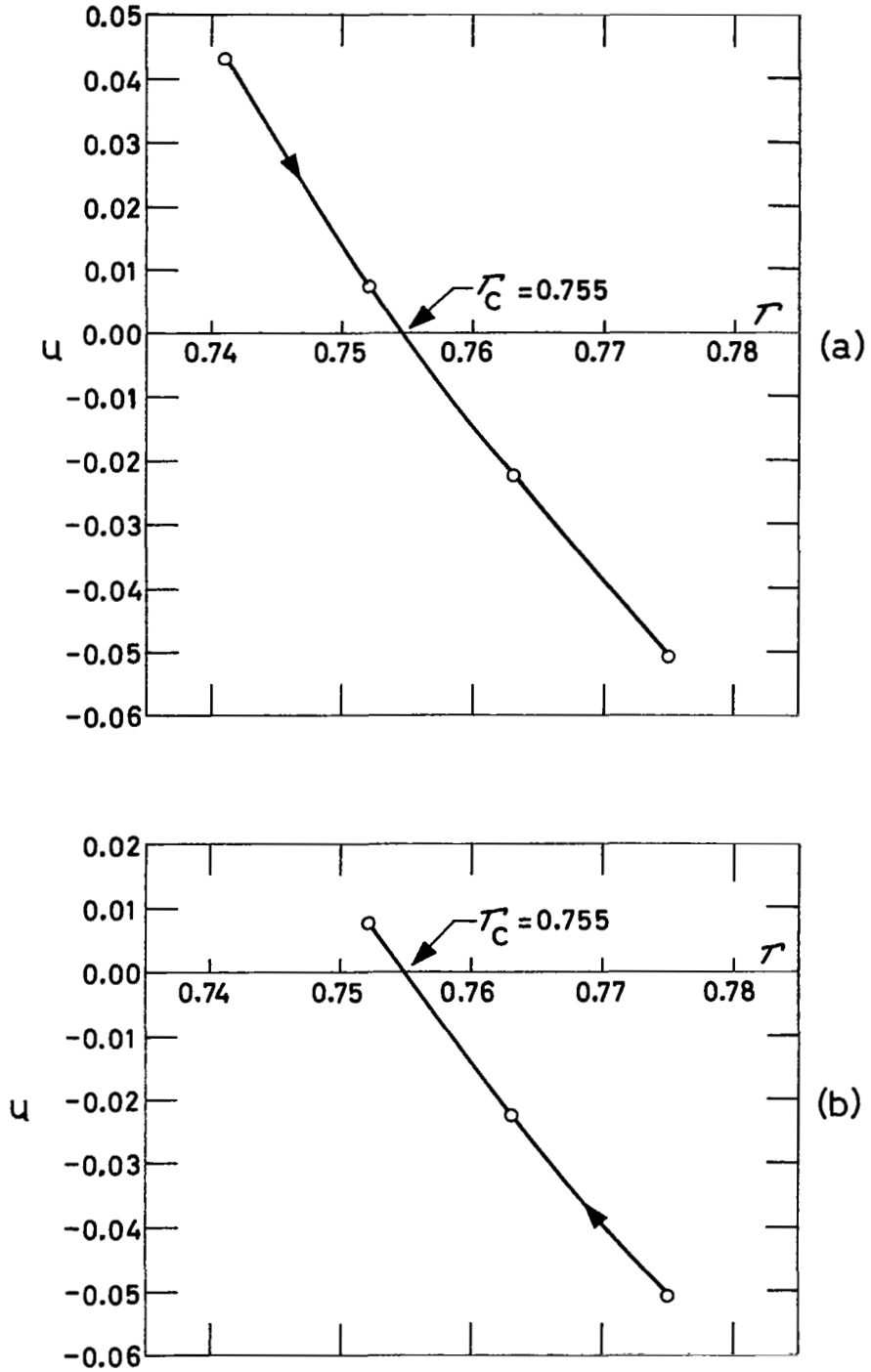

Figure 9: Steady State Centerline Velocity at the Location of the Incipient Breakdown (x = 0.75) as a Function of the Swirl Ratio for the Axial Inlet Stream Tube. Re = 100 and B = 8. (a) Initial Field Without a Vortex Breakdown. Swirl Ratio Increased. (b) Initial Field With a Vortex Breakdown. Swirl Ratio Decreased.

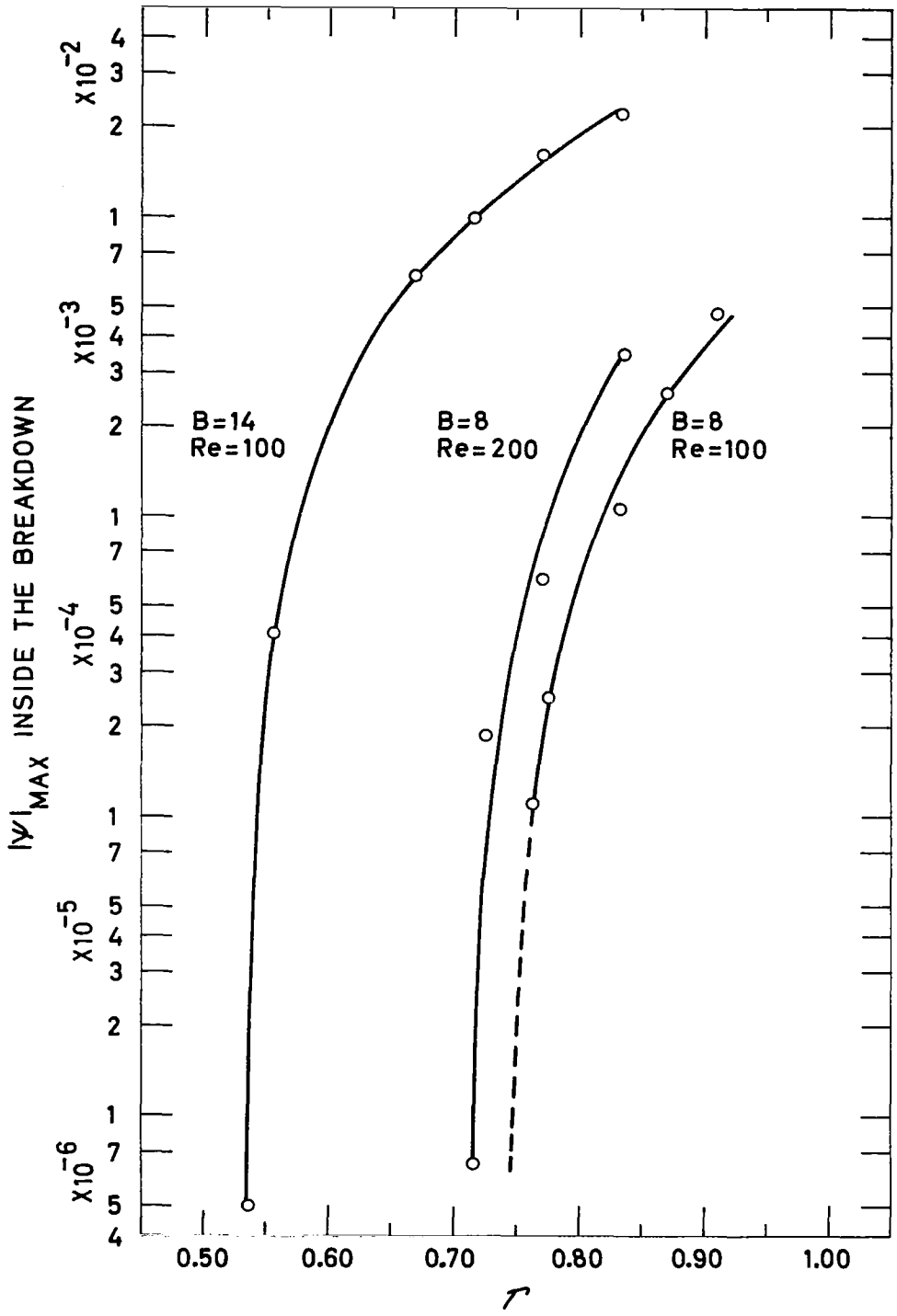

Figure 10: Maximum Absolute Value of Stream Function Inside the Breakdown for Various Values of Swirl Ratio. Axial Inlet Stream Tube Used.

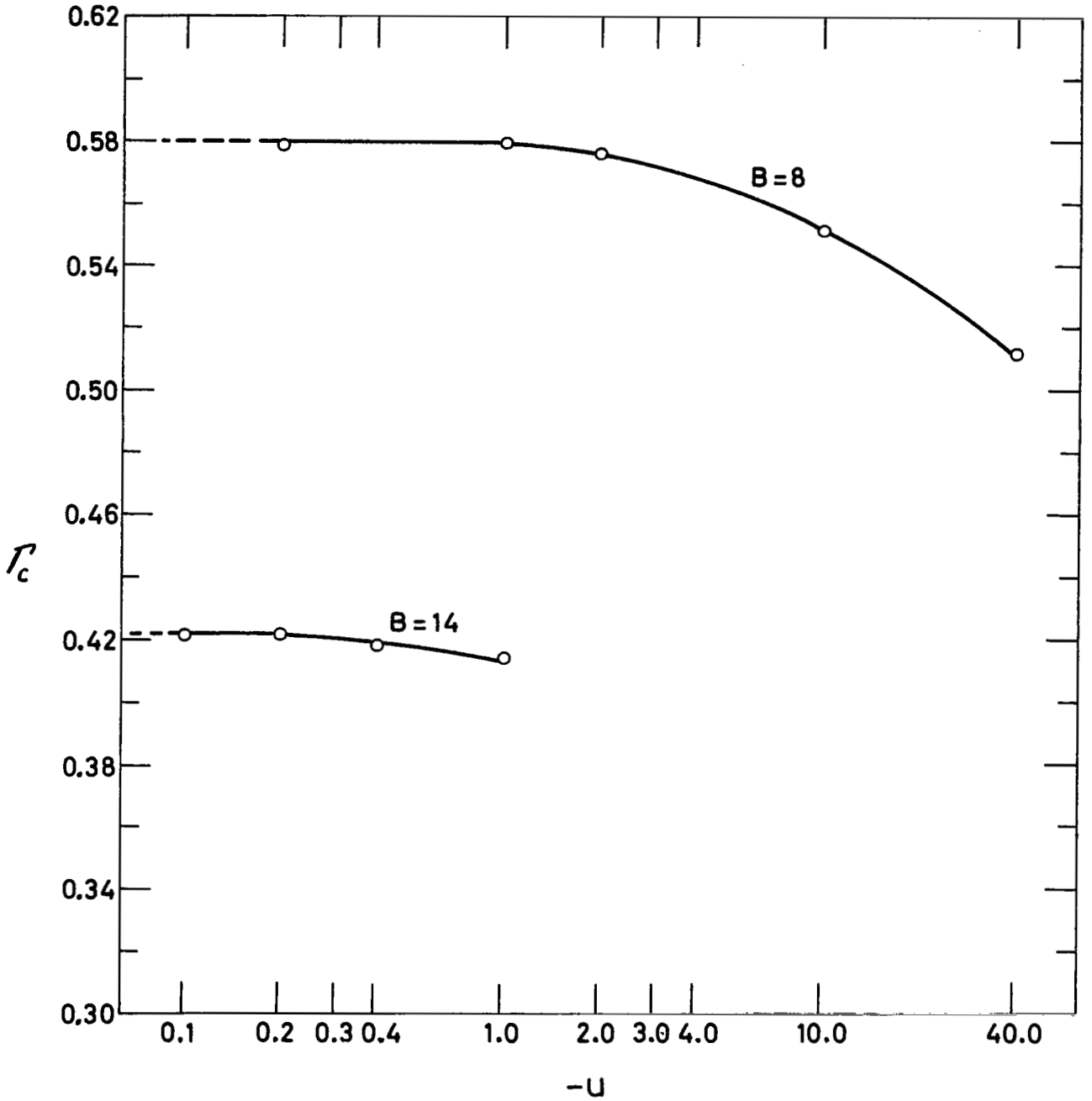

Figure 11: Critical Swirl Ratios for Various Size Negative Velocity Disturbances in an Inviscid Fluid. Axial Inlet Streamtube Used. Disturbances Introduced at x = 2.50, r = 0.

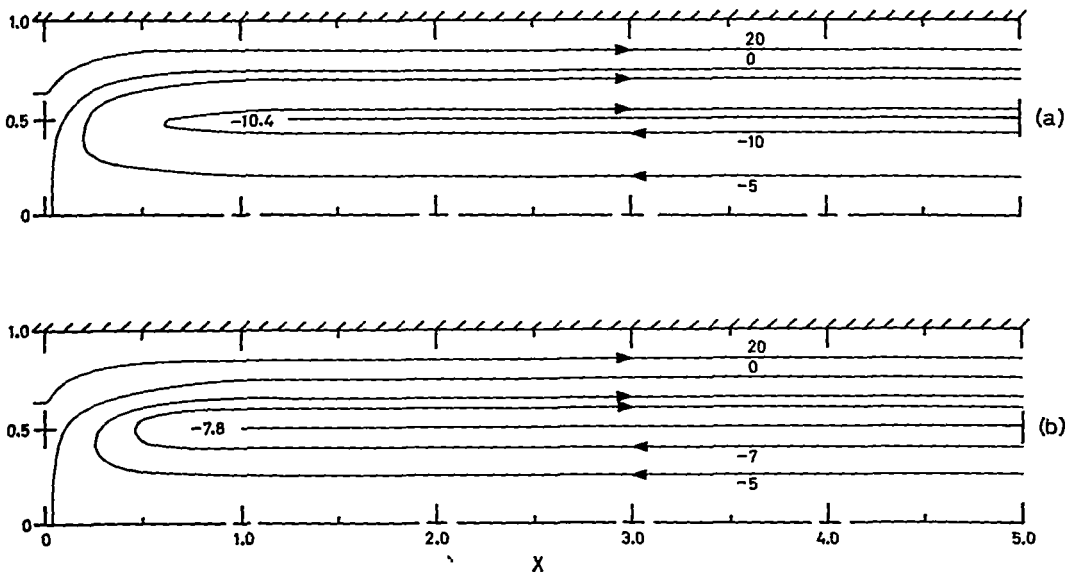

Figure 12: Incipient Vortex Breakdown in an Inviscid Fluid for the Axial Inlet Configuration. Stream Function Values Equal Those Shown x 10^{-2}. (a) B = 8 and Γ = 0.585; (b) B = 14 and Γ = 0.424.

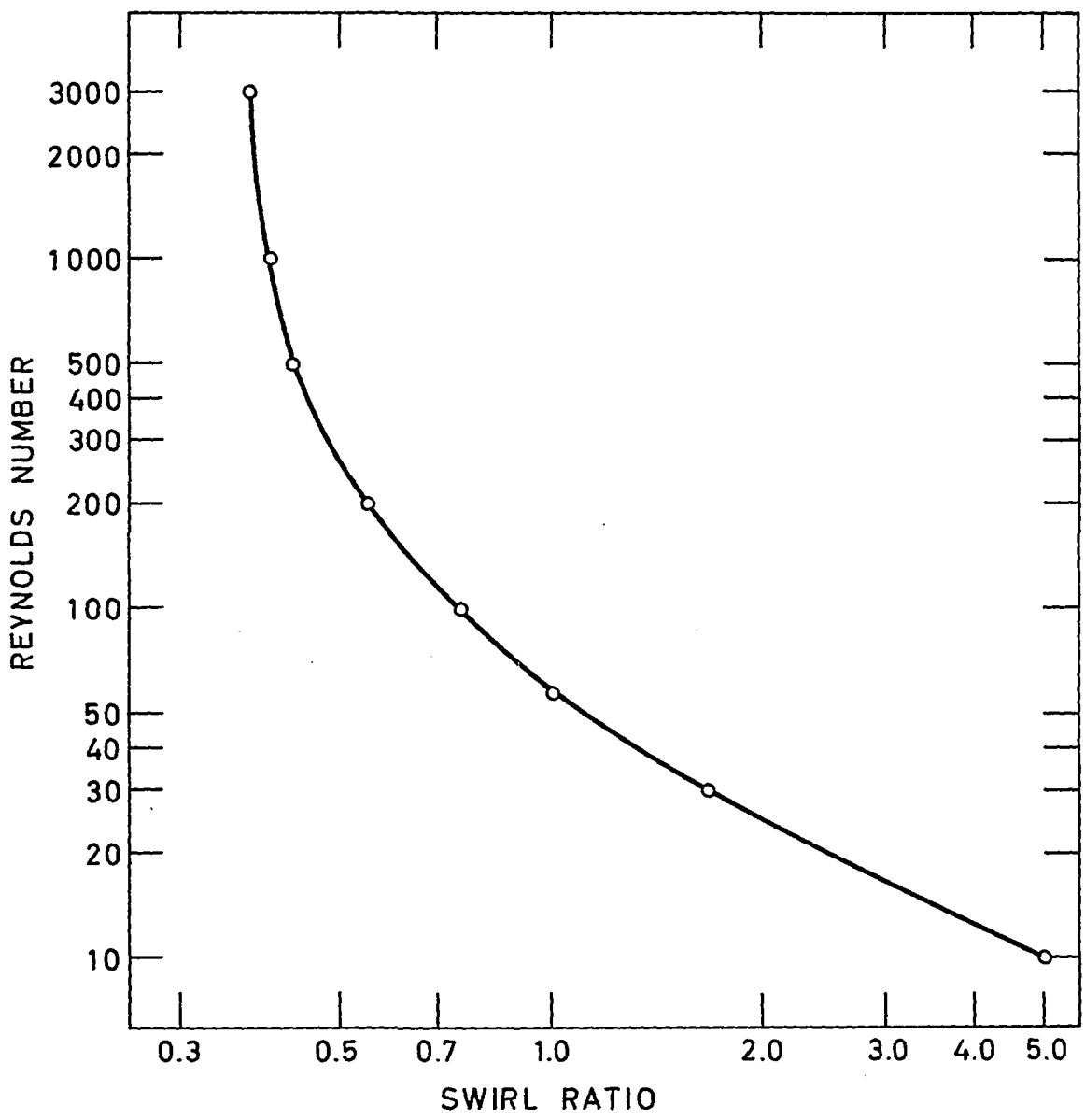

Figure 13: Swirl Ratios Required for an Incipient Breakdown at Various Reynolds Numbers for the Radial Inlet Stream Tube.

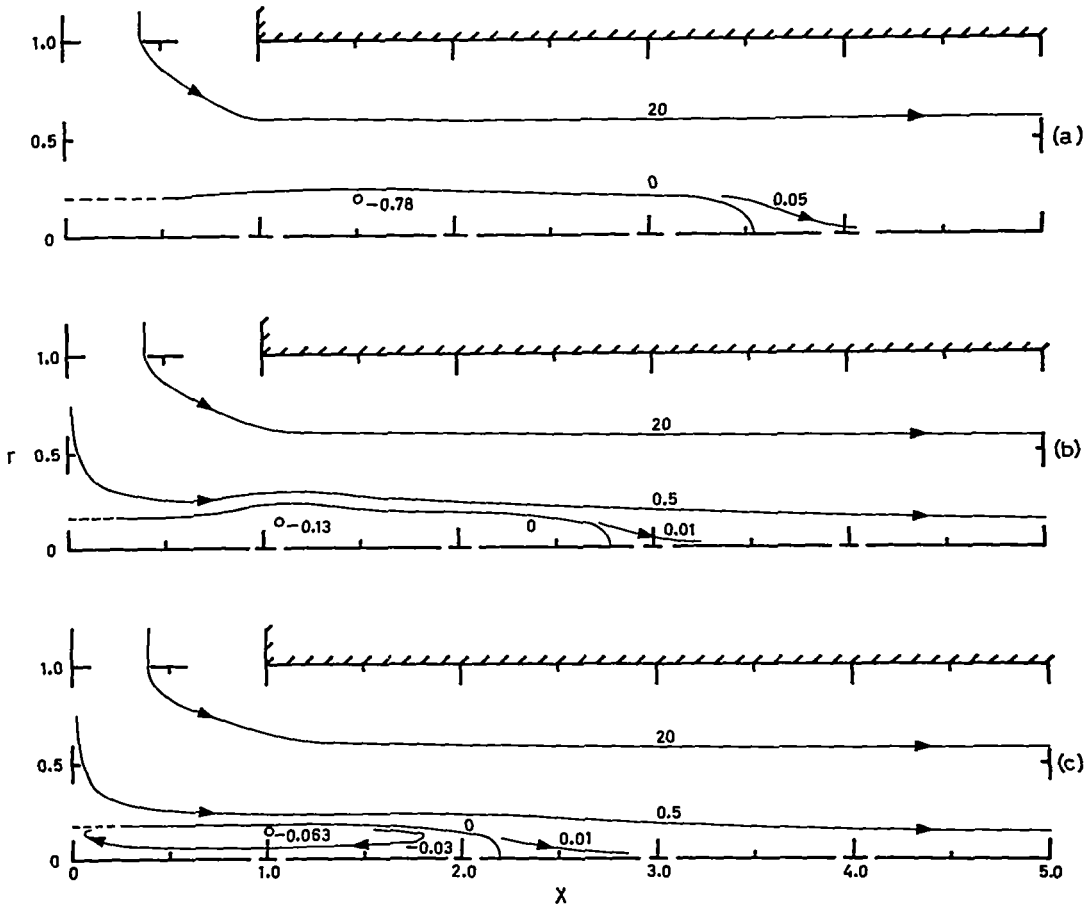

Figure 14: Vortex Breakdown for the Radial Inlet Configuration as Calculated Using Different Size Grids. Re = 100, Γ = 1.0. Stream Function Values Equal Those Shown x 10^{-2}. (a) 12 x 6 Uniform Grid; (b) 22 x 11 Uniform Grid; (c) 22 x 11 Variable Grid, Infinitely Long Tube.

NASA-Langley, 1971 —— 12 E-6326